Journal of Magnetism and Magnetic Materials 432 (2017) 472–476

Oxygen Pressure-Tuned Epitaxy and Magnetic Properties of Magnetite Thin Films

Junran Zhang,[1] Wenqing Liu,[2] Minhao Zhang,[1] Xaoqian zhang,[1] Wei Niu,[1] Ming Gao,[1] Xuefeng Wang,[1,a)] Jun Du,[3] Rong Zhang,[1] and Yongbing Xu[1,2,a)]

[1]*Jiangsu Provincial Key Laboratory of Advanced Photonic and Electronic Materials, Collaborative Innovation Center of Advanced Microstructures, School of Electronic Science and Engineering, Nanjing University, Nanjing 210093, China*

[2]*York-Nanjing Joint Centre (YNJC) for spintronics and nano engineering, Department of Electronics, The University of York, YO10 3DD, United Kingdom*

[3]*School of Physics, Nanjing University, Nanjing 210093, China*

Abstract

Quasi-two-dimensional Fe_3O_4 epitaxial thin films have been synthesized by pulsed laser deposition technique at six fixed oxygen pressures of 0, 1×10^{-5}, 5×10^{-5}, 1×10^{-4}, 5×10^{-4}, and 1×10^{-3} mbar. The film obtained under high vacuum ($\sim1\times10^{-8}$ mbar) hosts a large magnetoresistance of about 11.5 % at 9 T and 100 K. In addition, oxygen-pressure-dependent saturation magnetizations of the films are as large as that of the bulk Fe_3O_4. A trivial change in oxygen stoichiometry of Fe_3O_4 is found crucial for the ferrimagnetic order at room temperature. Possible mechanisms of ferrimagnetic order driven by change in oxygen stoichiometry are discussed.

Keywords:

Fe3O4 film, oxygen stoichiometry, magnetoresistance, magnetization, ferrimagnetic order

In the contemporary spintronics research, magnetite, especially in nano-form, has attracted enormous interest due to its great potential for information technology. To synthesize highly spin polarized materials as spin sources and to combine them with semiconductors, which can be easily integrated with current magnetic technologies are prerequisites for proposed spintronics devices such as the spin field effect transistor (SFET).[1] As a model half-metallic material, Fe_3O_4 has shown 80% spin polarization near the Fermi level in experiment[2] and theoretically, up to 100% can be expected.[3] More desirably, the high Curie temperature of Fe_3O_4 makes it a promising candidate for room temperature use. Fascinating properties of spin transport have also been presented in Fe_3O_4, i.e., spin Seebeck effect,[4] spin filter effect,[5] gate voltage-induced phase transition,[6] and spin valve effect of Fe_3O_4/MgO/Fe_3O_4 junctions.[7] Yet at the meantime, many fundamental properties of magnetite, such as the half-metallicity, spin and orbital ordering, Verwey transition mechanism and the coupling mechanism between different sites have long been open issues, and with the Fe_3O_4 synthesized under different oxygen pressure, these issues become even more sophisticated.

Magnetite is believed to have a cubic inverse spinel structure, where Fe^{3+} ions occupy tetrahedral sites (usually called A sites), whereas octahedral sites (B sites) are occupied by both Fe^{3+} and Fe^{2+} ions. The spin of Fe^{3+} ions at octahedral and tetrahedral sites are aligned antiparallel to each other leading to a net magnetic moment of 480 emu/g (4 μB/f.u.), corresponding to a fully occupied local majority band (opposite for A and B sites). The presence of integer magnetic moment of magnetite is expected in experiment as indication for a B-site minority electron conduction mechanism, and its accompanied full spin polarization at the Fermi level. However, controversial results of it have been reported varies from 300 emu/g by Nagahama *et al.* using molecular beam epitaxy (MBE) under oxygen pressure[8] to 1094 emu/g by Orna *et al.* using pulsed laser deposition (PLD) under pure vaccum.[9] Table I summaries some of the experimental efforts toward this issue.

Over the one-century's research on magnetite, there exists wide-spread recognition that further insights into open problems relating to magnetite are obtainable only by means of bulk, single crystals of perfect stoichiometry, grown in accordance with optimum preparation rules and phase diagrams. This, in one respect, strongly depends on the accurate controlling of the oxygen pressure, not only during maintenance of the thermodynamic high-temperature equilibrium, but also-most importantly-during cooling down to room-temperature. Violation of this precept-by uncontrolled quenching of the sample, as is often practiced at the end of tempering-causes considerable loss of crystal quality, as shown in several reports.[9-14] The magnetization of Fe_3O_4 thin films grown by PLD can be tuning by oxygen partial from 0.4×10^{-6} to 10×10^{-6} Torr.[10] Seki *et al*. grew Ge-substituted Fe_3O_4 thin films under high oxygen pressures (0.01-0.6 Pa) and yielded a spin polarization of 0.50 at room temperatur.[11] However, Fe_3O_4 epitaxial thin films with giant magnetic moment, which comes from the spin of Fe ions

in the tetrahedron site switching parallel to the Fe ions in the octahedron site at the surface, interface, and grain boundaries, were grown in pure vacuum by PLD.[9,15] The influence of oxygen pressure on the quality of Fe_3O_4 thin film by PLD is unclear.

In this work, we present systematic investigation of oxygen-pressure-dependent magnetoresistance (MR) and magnetic moment, aiming to contribute to the open question of the magnetic moments of the Fe_3O_4 thin film. Quasi-two-dimensional (quasi-2D) Fe_3O_4 thin films (~100 nm) were deposited on MgO (001) substrates by PLD. First, a sharp MgO (001) surface was obtained after annealed in vacuum atmosphere for 8 hours at 600 ºC as identified from the reflection high-energy electron diffraction (RHEED) pattern shown in Fig. 1(a). The films were grown at about 410 ºC and six different fixed oxygen pressures atmosphere (0, 1×10^{-5}, 5×10^{-5}, 1×10^{-4}, 5×10^{-4}, and 1×10^{-3} mbar). Prior to film deposition, the chamber was pumped down to ~1×10^{-8} mbar. *In situ* and *real time* monitoring of the growth was performed by RHEED. All films were characterized by X-ray photoelectron spectroscopy (XPS, PHI 5000 VersaProbe), and laser Raman spectrometer (JY HR800). MR and resistance-temperature (R-T) curves were measured by Physical Property Measurement System (PPMS, Quantum Design, Inc.). The magnetic properties of the samples were measured at room temperature using a vibrating sample magnetometer (VSM).

The dot-array and long-line-array in RHEED patterns stand for three dimension (3D) and quasi-2D surface structure and morphology, respectively.[16] Fe_3O_4/MgO with quasi-2D surface structure and morphology was shown in Fig. 1(b), which reveals that the surface quality of our Fe_3O_4 thin films prepared by PLD is as high as films grown by MBE.[17,18] Due to the fact that the lattice constant of Fe_3O_4 (a=8.3987 Å) is twice of MgO (a=4.212 Å),[19] the emerging patterns of line 2 and 4 in the middle of line 1,3 and 5 are pattern of Fe_3O_4. In order to study the surface structure of Fe_3O_4 thin film depending on oxygen partial pressure, *in situ* and *real time* RHEED was monitoring during growth of the 6 samples. As we can see from Fig. 1(c), the distances ratio between line 2 and 3 from Fig. 1(b) are invariable and the line width of line 2 increased as oxygen pressure increasing. This means that the phase of Fe_3O_4 become weak as oxygen pressure increasing. These phenomena can be explained by some Fe_2O_3 phases generated as oxygen pressure increasing. In order to confirm the Fe_2O_3 phase, the XPS and Raman were investigated.

Fig. 2(a) is the XPS spectra of Fe_3O_4 thin films grown at six different oxygen pressures, inset is the enlargement of the area in dashed line box. The typical Fe $2p_{3/2}$ and Fe $2p_{1/2}$ are observed at ~710 and ~723 eV, respectively. It is known that FeO has a clear satellite feature at ~715.5 eV, and Fe_2O_3 has a satellite feature at ~719.1 eV. Such satellite structures are frequently used as fingerprints to identify the other iron oxide phases.[17] One can clearly see that with the exception of the sample grown at pure vacuum, the XPS spectra for all the other Fe_3O_4 thin films show signs for satellite structures of Fe_2O_3 phase and all films show no signs

for satellite structures of FeO phase. The intensity of the satellite structures of Fe_2O_3 phase become stronger as the oxygen pressure increasing. This phenomenon is not completely accord with the report by Liu *et al*.,[17] in which Fe_3O_4 thin films grown by MBE at 8 different oxygen partial pressure (from 1×10^{-5} to 5×10^{-8} mbar), and with the exception of sample grown at the low 5×10^{-8} mbar oxygen partial pressure shown the sign for FeO, all the other samples show no signs for Fe_2O_3 and FeO.

Raman is also investigated to confirm the Fe_2O_3 phase as shown in Fig. 2(b). Considering the space group O_h^7(Fd3m), theory predicts the following modes by proper irreducible representation:[20]

$$A_{1g} + E_g + T_{1g} + 3T_{2g} + 2A_{2u} + 2E_u + 5T_{1u} + 2T_{2u}.$$

The T_{1g}, A_{2u}, E_u, and T_{2u} are silent. Thus there are five Raman active modes (A_{1g}+E_g+3T_{2g}) and five infrared active modes ($5T_{1u}$). At room temperature, we observe three modes: the strongest A_{1g} mode at ~675 cm^{-1} and T_{2g}(2) and T_{2g}(3) modes at ~550 and ~320 cm^{-1}, respectively. This is corresponding with the reference.[21] However, with exception of sample grown at the pure vacuum, all other samples show the A_{1g} peaks of Fe_2O_3 at ~210 and 480 cm^{-1}.[22] XPS and Raman spectroscopies confirm formation of single magnetite phase for the low oxygen pressures and a mixed phase composed of Fe_3O_4 and Fe_2O_3 for the high pressure.

The magnetic transport properties of films were investigated, which schematic structure for magnetotransport measurements in Fe_3O_4 films is shown in Fig.3(a). The R-T of the films were measured as shown in Fig. 3(b). It can be see that a suddenly increase of the resistivity was observed at ~110 and ~124 K for Fe_3O_4 films grown at pure vacuum and oxygen partial pressure of 1×10^{-5} mbar, respectively, corresponding to the Verwey transition.[23] Inset of Fig 3(b) is log resistance versus the inverse temperature of Fe_3O_4 films grown at pure vacuum, which can see the Verwey transition obviously. At the same temperature, the resistance of Fe_3O_4 film grown at pure vacuum is smaller than Fe_3O_4 film grown at oxygen pressure of 1×10^{-5} mbar, which possibly attributed to the Fe_2O_3 phase generated due to oxygen partial pressure. Fig.3(c) and (d) show the MR measurements at different temperatures for the Fe_3O_4 thin films grow at pure vacuum and oxygen pressure of 1×10^{-5} mbar with the magnetic field applied perpendicular to the film plane. As we can see, a large MR value of 11.5 % at 100 K and 9 T is observed, which is larger than references reported.[24,25]

In spite of Fe_3O_4 thin films grown in oxygen pressures exist Fe_2O_3 phase, magnetic hysteresis loops are observed for all the samples as shown in Fig. 4. The hysteresis loops are obtained at room temperature for five of the samples. As we can see from Fig. 4(a), the large saturation magnetization (M_S) of 425 emu/cm^3 approaching at the principle bulk-like magnetite saturation value[26] (480 emu/cm^3 or 4.0 μ_B/f.u.) is observed by the sample grown at

pure vacuum, which is larger than Fe_3O_4 thin films reported by Arora *et al.*[27] and Orna *et al.*[9] with same thickness. The saturated magnetic moment decreased due to Fe_2O_3 impurities phase generated as increasing the pressure of oxygen as shown in Fig. 4(d), which is extracted from Fig. 4(a) and (b). Both coercivities of in plane and out plane are invariable as oxygen pressure increasing. Fig. 4(c) shows the loops measured in plane and out plane of sample grown at pure vacuum. It is can be seen that the sample exhibits an unobvious out of plane anisotropy, which reveal the high quality of our films.

Arora *et al.*[27] reveal that the noncompensation of spin moments between the tetrahedral and octahedral sublattices at the surface are inferred to be the main factor contributing to the observed enhanced magnetic moment. Orna *et al.*[9] reveal that the origin of the enhanced magnetic moment is not intrinsic to magnetite but due to the presence of Fe impurities in the MgO substrates. Oxygen vacancies on electronic structure also can enhance magnetic moment as reported by Jaffari *et al.*.[28] For Fe_3O_4 double exchange interaction between Fe^{3+} and Fe^{2+} in octahedral site leads key role which produces ferromagnetic component.[29] In addition, antiferromagnetic super-exchange interaction between octahedral Fe^{3+} and tetrahedral Fe^{3+} cancels each other, retaining net moment of Fe^{2+} to be 4 μB/f.u.. Recent density of states calculations suggests reduction of moment locally due to oxygen vacancies, although total moment of the crystal remains unchanged.[30] In the current studies surface effect is rather less effective because of significantly large film thickness (~100 nm).[31] Strain is one of the key parameters which can influence magnetization significantly for films including magnetite.[32,33] A significant compressive strain is developed at the sample substrate interface because of lattice mismatch between MgO and Fe_3O_4. The strain increases further with oxygen deficiency and it might be involved with the larger number of oxygen defects at the interface for low oxygen partial pressure. A small change in oxygen stoichiometry is suggested to be correlated to the modification and drives a significant change in ferrimagnetic order.

In summary, we have successfully grown the quasi-2D Fe_3O_4 epitaxial thin films at different oxygen pressures by PLD. XPS and Raman spectroscopies confirm formation of single Fe_3O_4 phase for the low oxygen pressures and a missed phase composed of Fe_3O_4 and Fe_2O_3 phase for the high oxygen pressures. Oxygen stoichiometry of Fe_3O_4 film is found vital for ferromagnetic order.

Acknowledgements

This work was supported by the National Key Projects for Basic Research of China (2014CB921100), the National Natural Science Foundation of China (11274003 and 61274102), the PAPD project, and the Fundamental Research Funds for the Central Universities.

Method	Substrate	Thickness	MR (%)	Oxygen Pressure (mbar)	M_s	Reference
PLD	MgO(100)	100 nm	11.5 %	Pure vaccum	425 emu/cm^3	Our work
PLD	GaAs(100)	-	22 %	Pure vaccum	430 emu/cm^3	[34]
PLD	ZnO/Al_2O_3(0001)	70 nm	-	Pure vaccum	380 emu/cm^3	[35]
PLD	$SrTiO_3$(001)	-	-	Pure vaccum	400 emu/cm^3	[13]
PLD	YSZ(111)	-	-	2×10^{-6}	400-460 emu/cm^3 480 (Anneal) emu/cm^3	[36]
PLD	SrTiO3(100)	>15 nm 3nm	-	Pure vaccum	Close to 480 emu/cm^3 1017 emu/cm^3	[15]
PLD	MgO(001)	>20nm 2.8nm	-	Pure vaccum	349±41 emu/cm^3 About 1094 emu/cm^3	[9]
PLD	MgO(100)	10 nm	3%	Adequate oxygen pressure	-	[37]
PLD	MgO(111) MgO(100)	40 nm	5% 12 %	7.8×10^{-6}	470 emu/cm^3 400 emu/cm^3	[25]
PLD	MgO/GaAs(100)	-	-	5×10^{-5}	400 emu/cm^3	[26]
PLD	Si(100)	-	-	0.4×10^{-6} 4×10^{-6}	0.45 μB/f.u. 0.2 μB/f.u.	[10]
MBE	MgO(100)	-	-	1×10^{-6}	300 emu/cm^3	[8]
MBE	MgO(001)	10 nm	0.3%	6.6×10^{-6}	-	[38]
MBE	MgO(001)	1.5 μm	-	Oxygen plasma	300 emu/cm^3	[39]
MBE	MgO(001)	60 nm	5%	Oxygen plasma	-	[40]
MBE	MgO(001)	5nm 20 nm	-	Oxygen plasma	922 emu/cm^3 613 emu/cm^3	[41]
MBE	GaN(0001)	6 nm 3nm	-	8×10^{-4}	450 emu/cm^3 350 emu/cm^3	[42]

TABLE 1. MR and M_s of Fe_3O_4 films grown at different conditions of our sample and those from the literatures.

References

[1] S. Datta and B. Das, Appl. Phys. Lett. **56**, 665 (1990).

[2] Y. S. Dedkov, U. Rüdiger, and G. Güntherodt, Phys. Rev. B **65**, 064417 (2002).

[3] V. Antonov, B. Harmon, and A. Yaresko, Phys. Rev. B **67**, 024417 (2003).

[4] R. Ramos, T. Kikkawa, K. Uchida, H. Adachi, I. Lucas, M. Aguirre, P. Algarabel, L. Morellón, S. Maekawa, and E. Saitoh, Appl. Phys. Lett. **102**, 072413 (2013).

[5] Z. M. Liao, Y. D. Li, J. Xu, J. M. Zhang, K. Xia, and D. P. Yu, Nano Lett. **6**, 1087 (2006).

[6] J. Gooth, R. Zierold, J. G. Gluschke, T. Boehnert, S. Edinger, S. Barth, and K. Nielsch, Appl. Phys. Lett. **102**, 073112 (2013).

[7] H. C. Wu, O. N. Mryasov, M. Abid, K. Radican, and I. V. Shvets, Sci. Rep. **3**, 1830 (2013).

[8] T. Nagahama, Y. Matsuda, K. Tate, T. Kawai, N. Takahashi, S. Hiratani, Y. Watanabe, T. Yanase, and T. Shimada, Appl. Phys. Lett. **105**, 102410 (2014).

[9] J. Orna, P. A. Algarabel, L. Morellón, J. A. Pardo, J. M. de Teresa, R. López Antón, F. Bartolomé, L. M. García, J. Bartolomé, J. C. Cezar, and A. Wildes, Phys. Rev. B **81,** 144420 (2010).

[10] K. Dey, A. Ghosh, P. Modak, A. Indra, S. Majumdar, and S. Giri, Appl. Phys. Lett. **105**, 142905 (2014).

[11] M. Seki, M. Takahashi, T. Ohshima, H. Yamahara, and H. Tabata, Appl. Phys. Lett. **103**, 212404 (2013).

[12] M. Ishikawa, H. Tanaka, and T. Kawai, Appl. Phys. Lett. **86**, 2504 (2005).

[13] Q.X. Zhu, M. Zheng, M.M. Yang, R.K. Zheng, Y. Wang, X.M. Li, and X. Shi, Appl. Phys. Lett. **105**, 241604 (2014).

[14] J. Dho, Appl. Phys. Lett. **106**, 202405 (2015).

[15] X. Guan, G. Zhou, W. Xue, Z. Quan, and X. Xu, APL Materials **4**, 036104 (2016).

[16] A. Ichimiya and P. I. Cohen, *Reflection high-energy electron diffraction*. (Cambridge University Press, 2004).

[17] X. H. Liu, A. D. Rata, C. F. Chang, A. C. Komarek, and L. H. Tjeng, Phys. Rev. B **90,** 125142 (2014).

[18] Z. Ding, B. L. Chen, J. H. Liang, J. Zhu, J. X. Li, and Y. Z. Wu, Phys. Rev. B **90,** 134424 (2014).

[19] D. Margulies, F. Parker, M. Rudee, F. Spada, J. Chapman, P. Aitchison, and A. Berkowitz, Phys. Rev. Lett. **79**, 5162 (1997).

[20] J. Verble, Phys. Rev. B **9**, 5236 (1974).

[21] D. M. Phase, S. Tiwari, R. Prakash, A. Dubey, V. G. Sathe, and R. J. Choudhary, J. Appl. Phys. **100**, 123703 (2006).

[22] C. Baratto, P. Lottici, D. Bersani, G. Antonioli, G. Gnappi, and A. Montenero, J. Sol-Gel Sci. Techn. **13**, 667 (1998).

[23] E. J. W. Verwey, Nature **114**, 327 (1939).

[24] A. Ramos, J.B. Moussy, M.J. Guittet, A. Bataille, M. Gautier-Soyer, M. Viret, C. Gatel, P. Bayle-Guillemaud, and E. Snoeck, J. Appl. Phys. **100**, 103902 (2006).

[25] O. Chichvarina, T. S. Herng, W. Xiao, X. Hong, and J. Ding, J. Appl Phys **117**, 17D722 (2015).

[26] W. Q. Liu, Y. B. Xu. P. K. J. Wong, N. J. Maltby, S. P. Li, X. F. Wang, J. Du, B. You, J. Wu, P. Bencok, and R. Zhang Appl. Phys. Lett. **104**, 142407 (2014).

[27] S. K. Arora, H.C. Wu, R. Choudhary, I. Shvets, O. Mryasov, H. Yao, and W. Ching, Phys. Rev. B **77**, 134443 (2008).

[28] G. H. Jaffari, A. K. Rumaiz, J. C. Woicik, and S. I. Shah, J. Appl. Phys. **111**, 093906 (2012).

[29] J. B. Moussy, J. Phys. D: Appl. Phys. **46**, 143001 (2013).

[30] R. Arras, L. Calmels, and B. Warot-Fonrose, Appl. Phys. Lett. **100**, 032403 (2012).

[31] M. Fonin, R. Pentcheva, Y. S. Dedkov, M. Sperlich, D. V. Vyalikh, M. Scheffler, U. Rüdiger, and G. Güntherodt, Phys. Rev. B **72**, 104436 (2005).

[32] S. Jain, A. Adeyeye, and D. Dai, J. Appl. Phys. **95**, 7237 (2004).

[33] A. Ghosh, K. Dey, S. Sabyasachi, A. Karmakar, S. Majumdar, and S. Giri, Appl. Phys. Lett. **103**, 052412 (2013).

[34] R. Prakash, R. J. Choudhary, L. S. Sharath Chandra, N. Lakshmi, and D. M. Phase, J. Phys.: Condensed Matter **19**, 486212 (2007).

[35] R. Master, R. J. Choudhary, and D. M. Phase, J. Appl. Phys. **108**, 103909 (2010).

[36] K. Matsuzaki, V. K. Lazarov, L. Lari, H. Hosono, and T. Susaki, J. Phys. D: Appl. Phys. **46**, 022001 (2013).

[37] T. Tsuchiya, K. Terabe, M. Ochi, T. Higuchi, M. Osada, Y. Yamashita, S. Ueda, and M. Aono, ACS Nano **10**, 1655 (2016).

[38] H.C. Wu, R. Ramos, R. G. S. Sofin, Z.M. Liao, M. Abid, and I. V. Shvets, Appl. Phys. Lett. **101**, 052402 (2012).

[39] J. J. Krebs, D. M. Lind, E. Lochner, K. A. Shaw, W. Portwine, and S. D. Berry, J. Appl. Phys. **75**, 6688 (1994).

[40] H. C. Wu, M. Abid, B. S. Chun, R. Ramos, O. N. Mryasov, and I. V. Shvets, Nano Lett **10**, 1132 (2010).

[41] S. K. Arora, H.C. Wu, R. J. Choudhary, I. V. Shvets, O. N. Mryasov, H. Yao, and W. Y. Ching, Phys Rev B **77,** 134443 (2008).

[42] P. K. J. Wong, W. Zhang, X. G. Cui, Y. B. Xu, J. Wu, Z. K. Tao, X. Li, Z. L. Xie, R. Zhang, and G. van der Laan, Phys. Rev. B **81,** 035419 (2010).

Figure caption

Fig. 1. (a) RHEED pattern of MgO (100) substrate with quasi-2D surface structure. (b) RHEED pattern of Fe_3O_4/MgO grown at high vacuum (~1×10^{-8} mbar) with quasi-2D surface structure. The new pattern of line 2 and 4 representing the growth of Fe_3O_4. (c) The distance ratio between line 2 and 3 from (b) and the line width of line 2 depending on different oxygen pressure.

Fig. 2. (a) XPS and (b) Raman spectra of Fe_3O_4 films grown under different oxygen pressures. Inset of (a) is the enlarged view of dotted box.

Fig. 3. (a) The schematic structure for magnetotransport measurements in Fe_3O_4 films. (b) Resistance versus temperature of Fe_3O_4 films grown at pure vacuum and oxygen pressure of 1×10^{-5} mbar. Inset is the log resistance versus inverse of temperature Fe_3O_4 films grown at pure vacuum. (c) Magnetoresistance versus magnetic field of Fe_3O_4 film grown at pure vacuum. (d) Magnetoresistance versus magnetic field of Fe_3O_4 film grown at oxygen pressure of 1×10^{-5} mbar.

Fig. 4. In plane (a) and out plane (b) magnetic hysteresis loops of Fe_3O_4 films grown at different oxygen pressures measured at room temperature. (c) In plane and out plane loops of Fe_3O_4 films grown at pure vacuum. (d) Saturated magnetic moment and coercivity extract from (a) and (b).

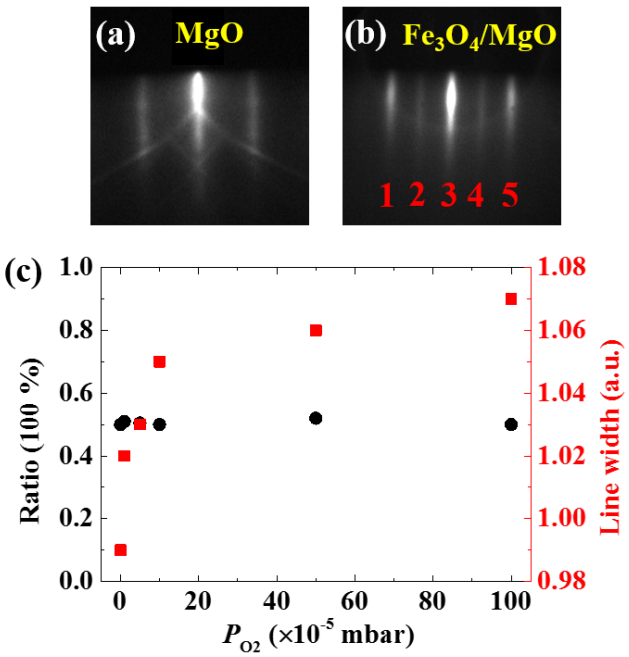

Fig. 1.

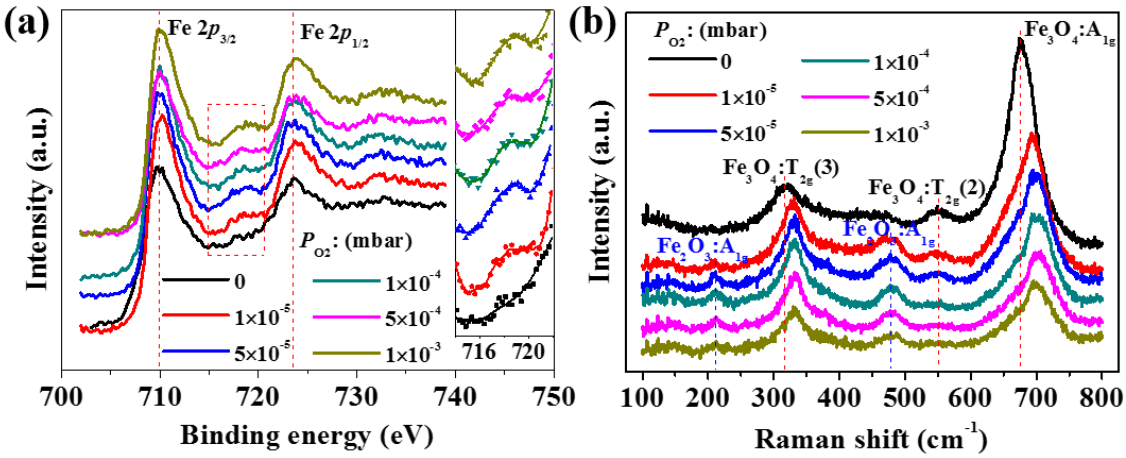
(a)
Fe 2p3/2
Fe 2p1/2
Intensity (a.u.)
PO2: (mbar)
0
1×10-5
5×10-5
1×10-4
5×10-4
1×10-3
716 720
700 710 720 730 740 750
Binding energy (eV)
(b)
PO2: (mbar)
Fe3O4:A1g
Fe3O4:T2g(3)
Fe3O4:T2g(2)
Fe2O3:A1g
Intensity (a.u.)
100 200 300 400 500 600 700 800
Raman shift (cm-1)

Fig. 2.

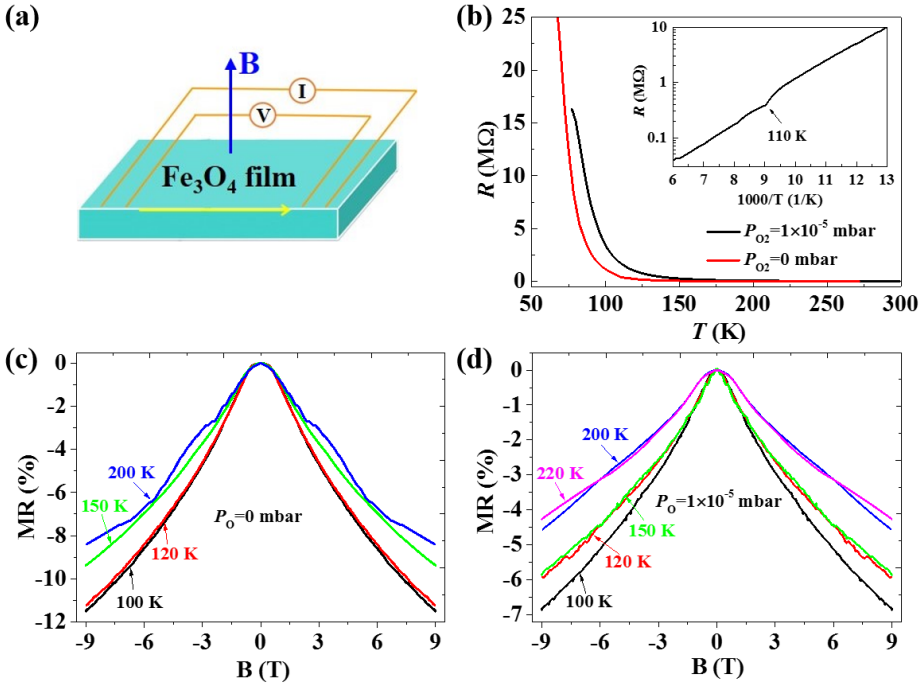
(a)
B
I
V
Fe3O4 film
(b)
R (MΩ)
T (K)
R (MΩ)
110 K
1000/T (1/K)
PO2=1×10-5 mbar
PO2=0 mbar
(c)
MR (%)
200 K
150 K
120 K
100 K
PO=0 mbar
B (T)
(d)
MR (%)
200 K
220 K
150 K
120 K
100 K
PO=1×10-5 mbar
B (T)

Fig. 3.

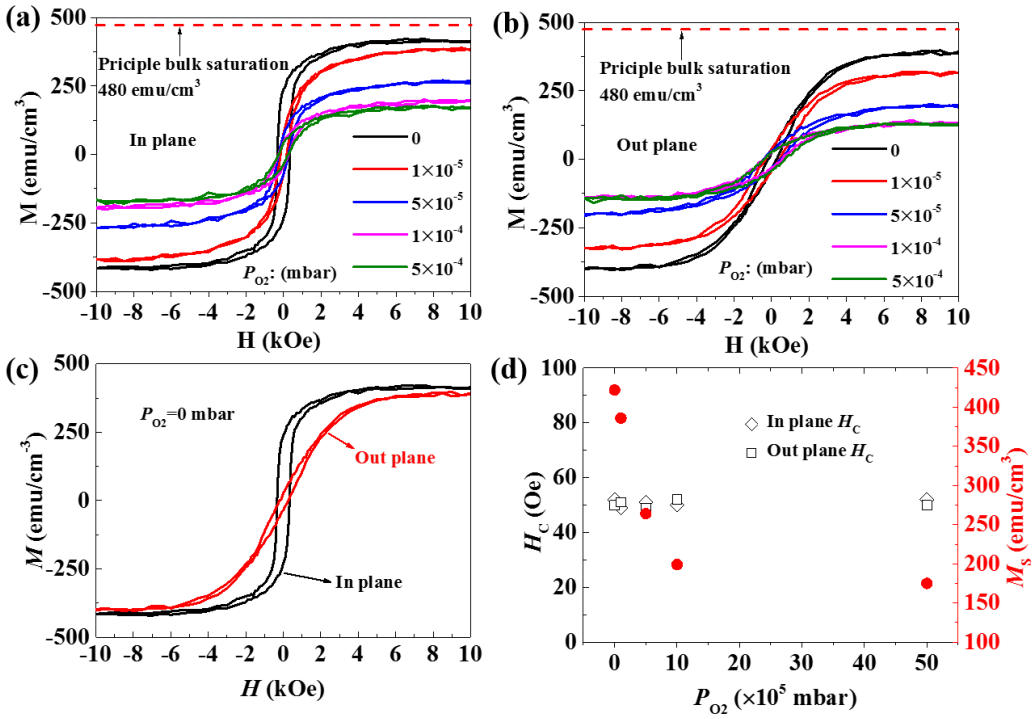
(a)
Priciple bulk saturation
480 emu/cm3
In plane
M (emu/cm3)
H (kOe)
P O2: (mbar)
0
1×10-5
5×10-5
1×10-4
5×10-4
(b)
Priciple bulk saturation
480 emu/cm3
Out plane
M (emu/cm3)
H (kOe)
P O2: (mbar)
0
1×10-5
5×10-5
1×10-4
5×10-4
(c)
P O2=0 mbar
Out plane
In plane
M (emu/cm-3)
H (kOe)
(d)
In plane HC
Out plane HC
HC (Oe)
MS (emu/cm3)
P O2 (×10^5 mbar)

Fig. 4.